Development and validation of analytical solutions for earth basket (spiral) heat exchangers

H.J.L. Witte[1], F. A. Heinrichs[2], C. Reichl[2], C. Meeng[1] , C. Doerr[2], A. Steurer[2], S. Kling[2],

1: Groenholland Geo-energysystems BV, Valschermkade 26, 1059CD Amsterdam, The Netherlands. Corresponding author: henk.witte@groenholland.nl

2: AIT Austrian Institute of Technology. Giefinggasse 2, 1210 Vienna, Austria.

henk.witte@groenholland.nl

Keywords: spiral ground heat exchanger, finite line source, g-function, computational fluid dynamics, model validation.

ABSTRACT

In this paper we present an analytical solution and its validation for earth basket (vertical spiral) ground heat exchangers. The model, based on the well known Finite Line Source Equation, accounts for the heat exchanger pipe diameter and seasonally varying near surface temperature. For computational efficiency the standard approach of using G-functions has been implemented as well. The analytical model is validated based on laboratory experiments and extensive CFD analysis.

SYMBOLS

d:	Distance (m)
P:	Point
P_o:	Point on outer GHEX pipe wall
P_i:	Point on inner GHEX pipe wall
x, y, z:	Coordinates in Cartesian space
R:	Average ring radius (m)
r:	GHEX pipe radius (m)
m, n:	GHEX Ring index
ω, φ:	Angular parameter (rad)
ΔT:	Temperature change (K)
t:	Time (s)
erf:	Error function
λ:	Thermal conductivity (W/mK)
α:	Thermal diffusivity (m²/s)
h:	Buried depth (m)
q':	Heat flux per unit length (W/m)

---

1. INTRODUCTION

Within the framework of the H2020 project "Geofit" (Eu grant no. 792210, www.geofit-project.eu) an integrated design toolbox for ground heat exchangers has been developed. Different types of ground heat exchangers exist, such as vertical borehole heat exchangers, horizontal heat exchangers, horizontal slinky heat[1] exchangers and so-called earth-basket or spiral heat exchangers. So far, no integrated toolkit to design all these different types of ground heat exchangers is available.

In Europe the commonly used design software (Earth Energy Designer, Blomberg et al. 2019) only allows the design of vertical borehole heat exchangers. In the USA design software was developed (GLHEPro, Spitler 2000) that allows the design of vertical boreholes, horizontal and slinky[1] type heat exchangers, but does not include a solution for vertical spiral type heat exchangers such as the so-called "earth basket" heat exchangers. Other existing engineering design software suites are equally limited in scope.

Spiral or coil heat exchangers have received attention in literature especially in the application in pile (foundation) heat exchangers (Cui et al, 2011; Man et al, 2011; Lei et al, 2018) as well as in horizontally oriented spiral heat exchangers (Wang et al, 2016). These models may ignore the inner-pile region (treating the pile as hollow). Moreover, the thermal properties of the pile are very different from the thermal properties of the ground. Therefore, these models are less suited for vertically oriented spiral heat exchangers installed not in foundation piles but directly in the ground, especially when the spiral (ring) diameter is relatively large as in earth basket heat exchangers.

According to Park et al (2013) the ring coil source model (Cui et al, 2011) and spiral heat source model (Man et al, 2011) do not provide an exact solution to the spiral coil source, have a singularity at $1/(t-t')^{3/2}$ and

---

requiring double integrations. They develop an improved three dimensional spiral coil analytical solution based on Green's function method.

Li et al (2012) describe a solution for a Slinky[tm] heat exchanger, consisting of series of rings in a horizontal plane, based on a ring source in an infinite medium. They obtain the temperature change of a ring source by integrating all contributions of point sources on the ring circumference. The point source solutions are obtained by applying Green's function. Mirror sources are used to obtain a isothermal surface boundary condition. Solutions for multiple ring cases are then obtained by superposition of the solution of the individual rings.

Xiong et al (2015) significantly improved the analytical models used for simulation of Slinky[tm] heat exchangers by considering the heat exchanger tube diameter and introducing a G-function approach to improve computational efficiency.

In this paper we extend the essentially two dimensional model developed by Xiong et al (2015) for horizontally and vertically oriented Slinky[tm] ground heat exchangers to a three dimensional solution for groups of vertically oriented spiral heat exchangers. A single spiral heat exchanger is represented by a series (stack) of ring sources, that are all separated by a certain distance (pitch). Several spiral heat exchangers can be installed in a single system.

The analytical model is extensively validated based on laboratory sand-box experiments and CFD analysis.

To increase computational efficiency the G-function approach (Eskilson, 1987) is used, but direct calculation is also possible. The solution has been implemented, together with solutions for vertical boreholes, horizontal heat exchangers and slinky heat exchangers, in a consolidated engineering tool implemented in the python programming language. Additional features implemented in the engineering toolkit are:

- Inclusion of near-surface seasonal temperature effects.
- Consideration of temperature dependent fluid properties, this is especially relevant for the fluid to ground thermal resistance calculations.
- Implementation of a detailed thermal resistance model and evaluation of critical Reynolds numbers for different geometries, definition of transition zones from laminar to turbulent flow.
- Consideration of the hermal interactions between neighbouring systems.

Laboratory validation is based on sand-box experiments on spiral heat exchanger configurations in a controlled environment. Temperature response of several different configurations were measured and used to validate a detailed numerical model. Using the model other configurations and heat rates could be evaluated that were then used for the validation of the FLS model (Kling et al 2022).

The laboratory experiments, CFD computations and FLS model were then used in a performance analysis study to investigate which parameters were suited for optimization and generate guidelines for engineers in selection of pipe diameters, ring diameters and pitches depending on the operational characteristics of the system being designed. Currently long term far field simulations are also underway to further validate and analyse the thermal behaviour of earth basket spiral heat exchangers. Early results indicate that for a set of ground heat exchangers their spatial arrangement is a key parameter both for their performance and also for their interaction with the surrounding media.

In the Bordeaux demo site (IUT Civil Engineering, Student Laboratory) two earth basket spiral type heat exchangers were installed and coupled to a prototype heat pump system (figure 1). Temperature measurements using a fibre optic distributed temperature sensing methodology are being carried out for further analysis of the earth basket heat exchanger performance and comparison with simulations.

Figure 1: Earth basket spiral type heat exchanger installed at the IUT Civil Engineering, Student Laboratory (Bordeaux, France) pilot site.

2. METHODOLOGY

Finite Line Source Solution for earth basket spiral heat exchangers

The fundamental equation to calculate the temperature response at a certain distance from the ground heat exchanger used in this study is the Finite Line Source (FLS) equation (Eskilson, 1987). The FLS has been used extensively to calculate the thermal response of different types of ground heat exchangers. For instance Cimmino (2013) recently improved the FLS for vertical

borehole heat exchangers while Xiong et al (2015) improved the FLS for ring-type Slinky^{tm} type heat exchangers. They include the heat exchanger tube diameter in the expression (especially relevant to calculate the temperature effect on the heat exchanger itself). In this paper we extend the solution presented by Xiong et al (2015) to three dimensions.

Figure 2 shows a top view of two horizontally oriented rings, For any point P on ring n with central coordinates x_n, y_n, z_n, the distance to a point P on ring m is given by:

$$d(P_n, P_m) = \frac{d(P_n, P_{om}) + d(P_n, P_{im})}{2} \qquad [1]$$

Here P_{om} is the coordinate of the point on the outer tube wall and P_{im} the point on the inner pipe wall, with distance expressed as:

$$d(\boldsymbol{P_n}, \boldsymbol{P_{om}}) = $$
$$\sqrt{\begin{array}{c} [x_n + \cos \omega - x_m - (R+r)\cos \varphi]^2 + \\ [y_n + R\sin \omega - y_m - (R+r)\sin \varphi]^2 + [z_n - z_m]^2 \end{array}}$$
$$[2]$$

$$d(\boldsymbol{P_n}, \boldsymbol{P_{im}}) = $$
$$\sqrt{\begin{array}{c} [x_n + \cos \omega - x_m - (R-r)\cos \varphi]^2 + \\ [y_n + R\sin \omega - y_m - (R-r)\sin \varphi]^2 + [z_n - z_m]^2 \end{array}}$$
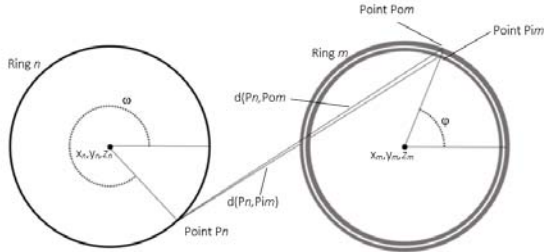$$[3]$$

Figure 2: Distance between points on two arbitrary rings (adapted from Xiong et al, 2015).

The principle of the FLS methodology is to define the geometry of the ground heat exchanger to be evaluated as a series of point sources with a constant energy flux and integrate over the geometrical shape. On the ground surface an isothermal temperature boundary condition is specified by defining mirror sources with an equal heat flux with opposite sign. In our implementation the earth basket spiral ground heat exchanger is simplified to a stack of rings with a constant distance (pitch) between the rings. Although this is a simplification of the actual helical geometry, the error introduced on the heat exchanger tube wall itself or at any significant distance is actually very small.
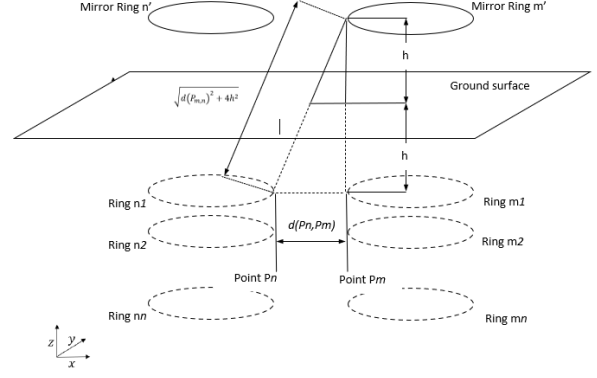

Figure 3: Simplified schematic of an earth basket spiral heat exchanger and it's mirror source (after Meeng, 2020).

Figure 3 shows a drawing of an earth basket spiral heat exchanger (with two separate earth basket spiral heat exchangers) with it's mirror source. The average tube wall temperature is calculated by superposition of all rings source with the temperature effect of a single ring source calculated by:

$$\Delta T_{m \to n}(t) = \frac{q'R}{8\pi^2 \lambda} \int_0^{2\pi} \int_0^{2\pi} \left[\frac{\text{erfc}\left(d(P_m, P_n)/2\sqrt{\alpha t}\right)}{d(P_m, P_n)} - \frac{\text{erfc}\left((d(P_m, P_n)+2h)/2\sqrt{\alpha t}\right)}{(d(P_m, P_n)+2h)} \right] d\omega d\varphi \qquad [4]$$

Using this solution and applying Eskilson methodology to obtain a G-function:

$$G_{eb}(t) = $$
$$\sum_{i=1}^{N_{ring}} \sum_{j=1}^{N_{ring}} \frac{R}{4\pi N_{ring}} \int_0^{2\pi} \int_0^{2\pi} \left[\frac{\text{erfc}\left(d(P_m, P_n)/2\sqrt{\alpha t}\right)}{d(P_m, P_n)} - \frac{\text{erfc}\left((d(P_m, P_n)+2h)/2\sqrt{\alpha t}\right)}{(d(P_m, P_n)+2h)} \right] d\omega d\varphi \qquad [5]$$

Experimental Setup and Temperature Measurement

For the study of the temperature response and validation of the CFD models sand-box experiments have been performed (see Kling, 2022, in these proceedings for a detailed discussion of the experiments). The experiment was set up in a HDPE plastic container with a total volume of 1 m^3 (Figure 4). To reduce experimental complexity the actual ground heat exchanger is represented by a heating cable. Advantages are that the heat pulse can be easily regulated and is constant over the complete length whereas a heat exchanger with circulating fluid would be difficult to control and would not offer constant heat flux per unit length.

In order to measure temperature gradients, a measuring system based on PT1000 sensors and a Distributed Temperature Sensing (DTS) system were installed inside the box.

Geometry and Mesh generation

A CFD model for the study of the earth basket spiral earth basket heat exchanger performance and validation of the analytical model has been developed in ANSYS FLUENT. The convergence behaviour of the CFD simulation highly depends on the quality of the mesh used in the calculation. On one hand, important heat flow details are to be precisely captured (requiring fine meshing), on the other hand the computing times shall be acceptable. The 3D domain of the soil and the heat exchanger are displayed by help of an unstructured mesh which allows a very high degree of flexibility. The element shape use tetrahedral cells. One of the most important factors to check the quality of the mesh is the skewness. It can be shown that a too high skewness leads to instabilities and lower accuracy. For practical applications it is recommended that the skewness factor does not exceed 0.9.

In terms of generating the mesh on the basis of the geometry, following indications are given, based on practical experiences. This information helps to keep the calculation effort within economical boundaries:
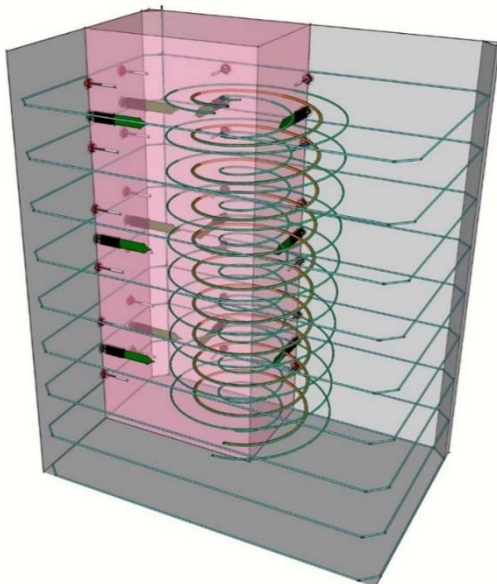

Figure 4: 3D sketch of the earth basket experiment's temperature sensor placement – the helix is shown in orange

- Maximum number of ten equilateral triangles to describe the circle of the heating cable in the XZ- plane
- Better resolution near the helix than in boundary regions of the box because of the temperature gradient being expected
- Wall-boundary cells may be bigger sized within limits of 50 to 100mm per cell
- As a rough estimation the number of cells should not exceed one million

These requirements suggest the application of a growth factor, starting with small elements on the helix with increasing element size towards the walls. Different growth rates are tested to show the (in)dependence of simulation results and growth rate. As smaller growth-rate leads to a significantly higher number of elements. Therefore a good compromise between accuracy and calculation effort has to be chosen.

Furthermore local mesh-refinement on specific points in the mesh is performed to reduce a potential dependency of the numeric solution regarding element size. The 3D-mesh consists out of tetrahedron elements while surfaces are meshed by help of triangle elements. The mesh has the following important element characteristics:

- Element size (wall sides) = 50mm
- Element size(top, bottom) = 30mm
- Element size(helix = heating cable) = 1.85mm

As element size is getting greater from small sized elements on the heating cable (helix) to the walls of the cubic box. The following growth rate is implemented into ANSYS due to a good compromise between accuracy and calculation effort: - using a growth rate of 1.9, a mesh consisting of 1 041 740 elements has been generated for the comparison to experimental data. For the comparison to the finite line source model the helix has been placed into a box with increased distances to the side walls and to the bottom. To keep the number of elements at an acceptable number ($10 - 20 \cdot 10^6$) and better capture the curved geometry, the following mesh characteristics were used (mesh has 12 514 246 elements):

- Element size (wall sides) = 150mm
- Element size(top, bottom) = 150mm
- Element size(helix = heating cable) = 1mm
- Growth rate = 1.6

Figure 5 shows a grid view of the 3D mesh model and a detailed view on the heating cable. Figure 6 visualizes the grid refinement in the vicinity of the helix.
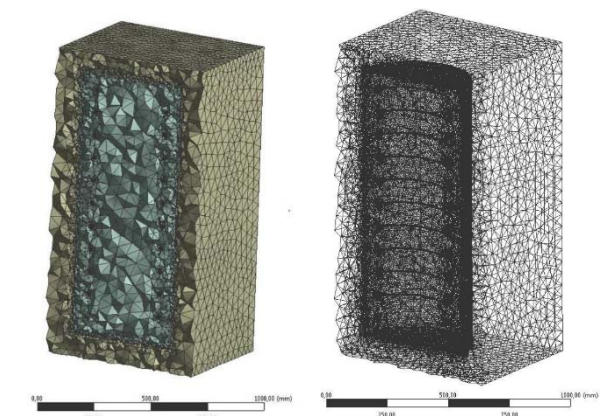

Figure 5: Grid view of the 3D mesh model (left) and zoom onto the heating cable (right)

CFD solution

To calculate the transient / steady temperature distribution, the Navier Stokes Solver Suite ANSYS Fluent was used.

To be able to compare to the experimental data set, the measured heating power value on the helix was used to generate a corresponding heat source in the simulation. Temperature dependent material parameters have been implemented according to the thermophysical properties of the soil used in the experiment for the comparison to the experimental data. Constant material properties have been used for the simulations, that are used for the comparison to the finite line source model. In all cases, the outer six walls of the box have been set to a fixed temperature of 283.15 K (10°C).

Figure 6: Mesh refinement on the heating cable

3. RESULTS

The construction parameters of the earth basket spiral heat exchanger used to perform the validations are given in table 1. These parameters were selected first to correspond with the sand-box experiments where the total heat injection was 113.1 Watts (10.24 W/m for the ring based solution). The buried depth in the sand box experiments was 0.16 m and, as the experiments were conducted in an climate chamber, the temperatures on the top, bottom and sides were fixed. As this is not possible for the FLS solution (only a constant temperature on the top surface boundary can be specified) the CFD model was adapted to include a larger domain as well as a realistic buried depth of 1.5 meters.

The helical fibre-optic cable next to the heat source is denoted as "Middle" and plotted in orange. The other two helical fibre-optic cables, with a radial distance of

75 mm to the heat source, are denoted as "Inner" and "Outer" and plotted in blue and green respectively.

The first validation performed was to validate (or calibrate) and develop the CFD model. Figure 7 shows the experimentally measured temperature (transparent) and the simulated data (bold) at the fibre-optic cable sensor positions at the thermal equilibrium reached at time t = 788 000 s, which approximates to 9 days.
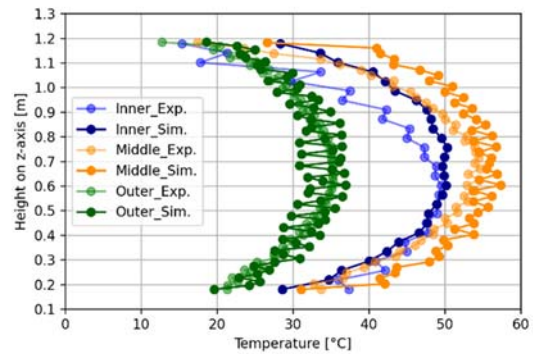

Figure 7: Simulation and experiment results form fibre-optic temperature sensors at steady state.

Overall, Figure 7 shows a good match between experiment and model. The best fit is at the centre of the model, while a slight deviation towards the boundaries at the top can be observed. This deviation in the upper half of the box may be credited to sand consolidation due to movement of the box. The rectangular shape of the box, in which the earth basket is placed, can be observed at the model's "Outer" fibre-optic temperature sensors. There is a stronger temperature difference between data points placed directly next to each other along the helical path of fibre optic cable, as the distance to the boundaries vary in x and y axis directions. This effect is the strongest on the "Outer" fibre-optic sensors, because the effect of the boundary conditions is stronger, as they are radially placed closer to the boundaries and experience lower temperatures
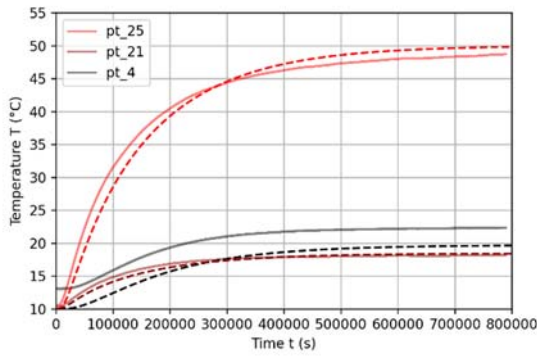
Figure 8: Transient earth basket simulation (- - -) and experiment (----) at three distinct RTD sensor positions

Additionally to the fibre-optic temperature sensors in the vicinity of the heat source, model and experiment are further compared at chosen RTD sensor positions. Three distinct sensor positions were chosen and compared in Figure 8. Sensor point "pt-25" is located exactly at the centre of the box, while the other two sensors "pt-4" and "pt-21" are located on the x and y axis respectively, at a medium height. Experimentally measured data is plotted in solid lines again, while the simulated results at the corresponding sensor positions are plotted in dashed lines. A rapid temperature increase with passing time can be observed in the early transient stage, while near steady-state conditions are clearly visible after approximately nine days. Initially, the temperature difference at the discussed RTD sensor positions in Figure 8 seem quite large. However, at time t = 0 s a distinct offset at all three sensor positions can be observed. This is due to the fact that in the experiment, the initial condition of 10 ∘C has not yet spread throughout the entire box.

A representation of the temperature field evolution calculated by CFD simulation at three different times is shown in Figure 9.
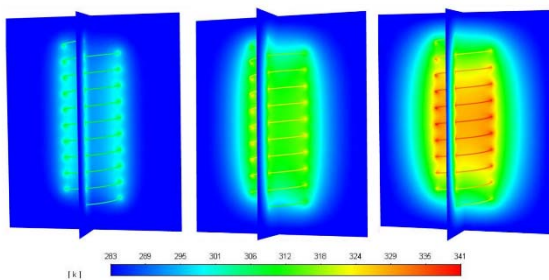

Figure 9: Contour plot of temperature at several time-steps in a transient simulation (left: 60000 s, middle: 180000 s, right: 840000 s)

Validation of the analytical FLS model

Reference values for the parameter variations used in the validation runs are given in table 2. For the

validation the heat injection rate, soil thermal conductivity, pitch and ring diameter were varied.

The comparison between the FLS solution and the CFD solution is made by comparison of the calculated temperatures at 182 distinct locations in the three dimensional space (Figure 10). In the Z-direction in total 14 levels have been defined. In the XY plane 13 distinct locations are used (Figure 11). Note that, although in the ring representation the points in the XY plane all have the same distance to the ring, this is not the case for the corresponding helical turn. For the simulations with different earth basket spiral heat exchanger diameters comparable distributions of the points for comparison were made.

Table 1: Overview of soil thermal parameters and earth basket spiral heat exchanger dimensions used for the validation.

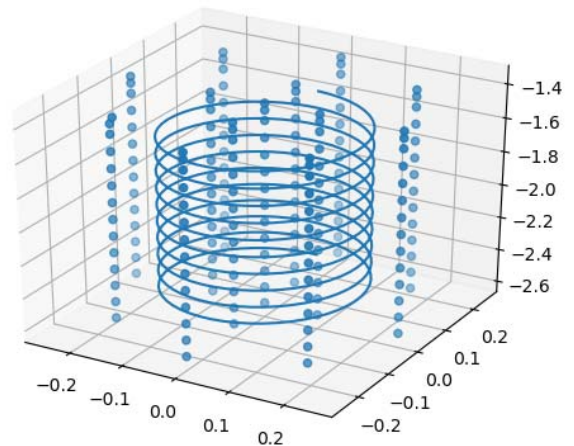| Parameter	Value
Soil thermal conductivity (W/mK)	2.0
Soil heat capacity (J/kgK)	2500
Soil density (kg/m^3)	1000
Soil temperature (ºC)	10.0
Buried depth (m)	1.5
Ring diameter (m)	0.35
Pipe outer diameter (m)	0.06
Number of rings	10
Total pipe length (m)	11.04
Pitch (m)	0.1
Thermal load (W/m)	10.24

Figure 10: 3D view of the helical coil and points used for comparison between FLS and CFD simulations.
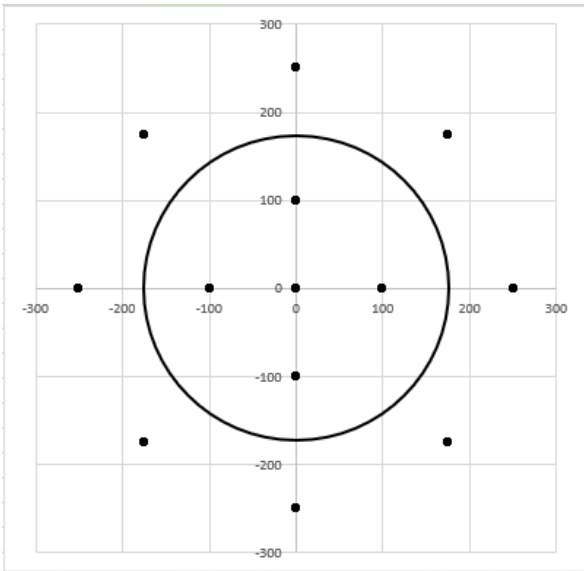
Figure 11: Top view of the ring (solid circle) and points used for comparison between FLS and CFD simulations (reference case).

The first question is how well the simplified geometry used in the FLS calculations, a simple stack of rings, approximates the actual helical geometry. Intuitively the average depth of one helical turn as Z-coordinate of the corresponding ring would seem the most logical choice.

To verify this calculations were performed for a one-ring situation with different buried depths. The average depth corresponding to the first ring is 1.55 meters (the helical coil starting at 1.50 meters below surface and ending at 1.60 meters below surface). The RMSE (root mean square error) between the CFD and FLS calculations are given in Figure 12. Clearly the smallest RMSE (0.062K) is achieved for the ring positioned at the average helical coil depth.

In this graph it can also be observed that the effect of the mirror source decreases with increasing depth, the RMSE for the deeper positioned ring is smaller than for the shallower positioned ring.

For the reference calculation with 10.24 W/m heat injection the temperatures for the CFD and FLS solution are shown in figure 13. Clearly there is a good match, the root mean square error is 0.25. Alternative plot of the CFD and FSL solutions directly with each other (Figure 14) shows a good linear fit between the two, the slope coefficient being very close to 1. This shows a good agreement between the reference case (experimental data, CFD and FLS simulations). Figure 14 shows a somewhat higher spread for low temperature changes (larger distance to heat exchanger spiral) and smaller spread for points with higher temperature change (closer to the heat exchanger).
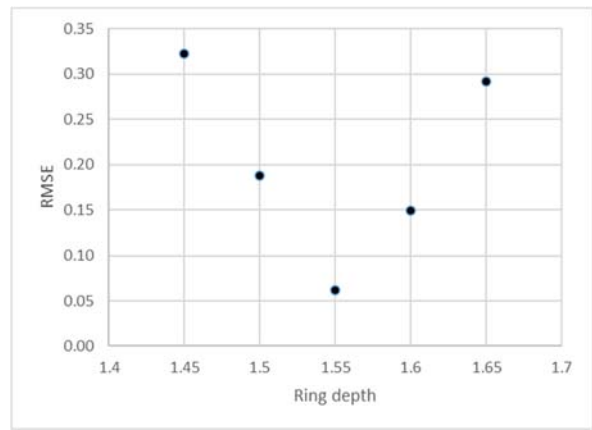

Figure 12: Comparison RMSE with different ring depths for the FLS solution, actual average buried depth for the helical coil is 1.55 meters.
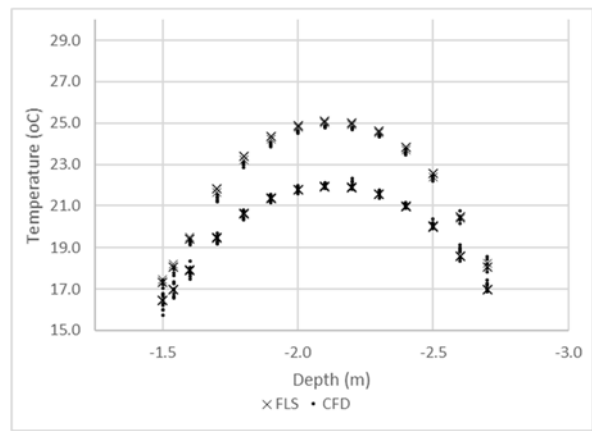

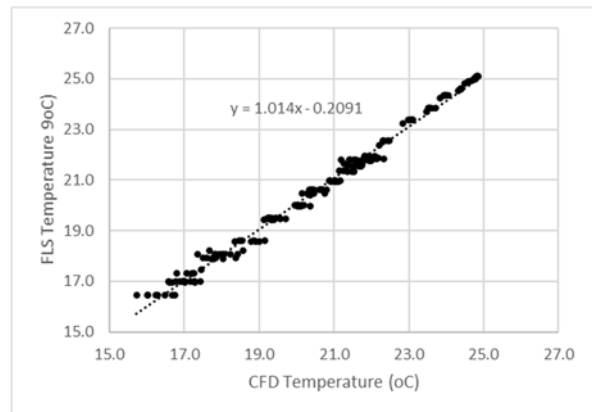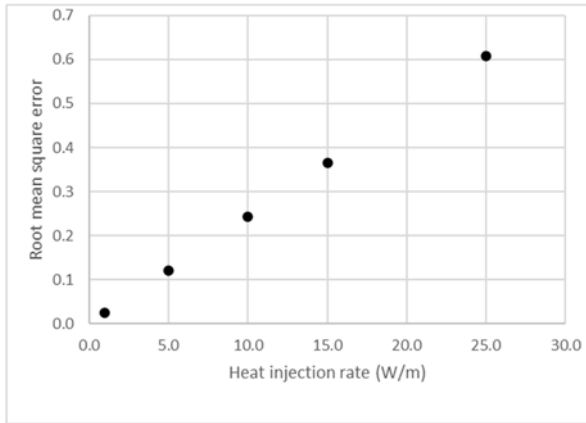**Figure 13: Temperatures calculated for the CFD and FLS solution, reference case**
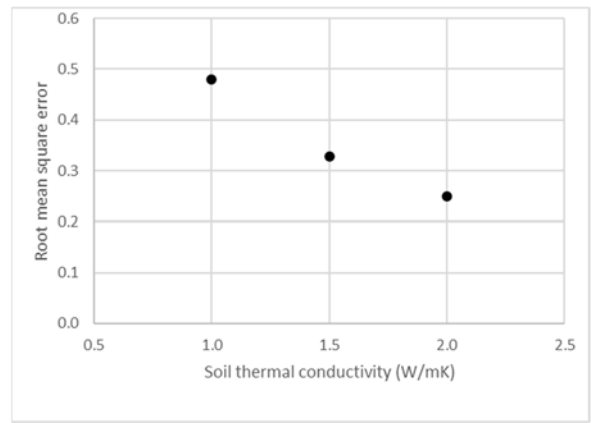

Figure 14: Temperatures calculated for the CFD and FLS solution, reference case.
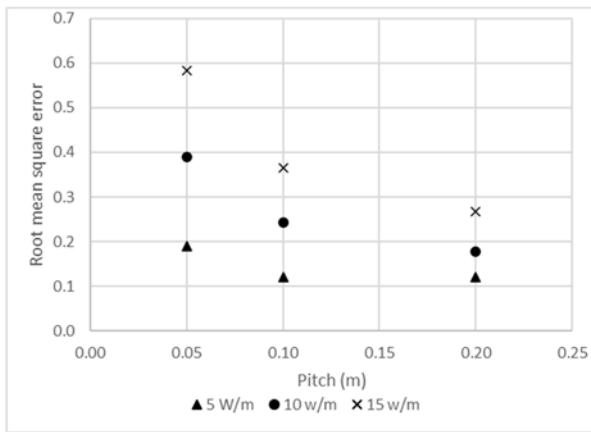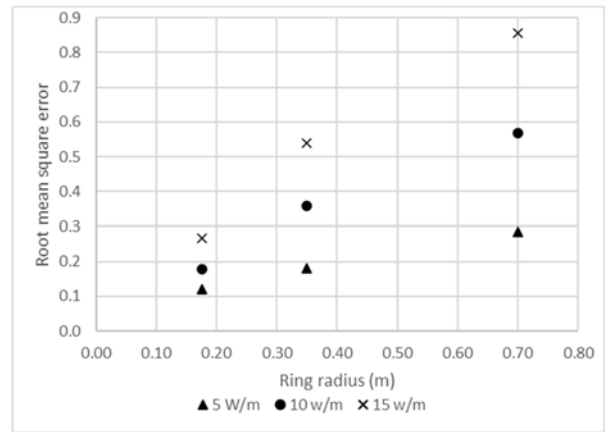
A

B

C

D

Figure 15: RMSE between CFD and FLS solution. 15A: variation of heat flux rates; 15B: variation of soil thermal conductivity; 15C: variation of pitch with different heat flux rates; 15D: variation of ring diameter with different heat flux rates.

After the initial validation, mainly comparison with experiment parameters and check on match between coordinate systems, further validations were performed where several parameters were varied:

- Specific heat flux (W/m): 1, 5, 10, 15, 25.
- Soil thermal conductivity (W/mK): 1.0, 1.5, 2.0.
- Pitch (m): 0.05, 0.10, 0.20, with 5, 10 and 15 W/m specific heat flux.
- Ring radius (m): 0.175, 0.350, 0.700 m, with 5, 10 and 15 W/m specific heat flux.

Figure 15 shows the results. All these simulations were performed for steady-state conditions.

If the RMSE is plotted as a function of the heat injection rate (figure 15A) there is clearly a linear relationship.

The maximum absolute error with an heat injection of 15 W/m is still only 0.3K, for the 25 W/m case the maximum absolute error for a single point is 1.8K.

The RMSE for the reference case and for the cases with different soil thermal conductivity is shown in Figure 15B. The RMSE ranges from 0.48 to 0.25 with the lowest RMSE for the highest soil thermal conductivity.

Analysis of different pitch for the heat exchanger (Figure 15C) shows a somewhat higher RMSE (0.36 – 0.58K) for the small pitch (0.05 m) and a small RMSE (0.17 – 0.27K) for the 0.2 m pitch. Variations of ring diameter (Figure 15 D) shows increasing RMSE with increasing ring diameter, RMSE 0.12 – 0.27K for 0.175 m ring diameter, 0.18 – 0.54K for 0.350 m ring diameter and 0.29 – 0.86K for 0.700 m ring diameter.

8

4. CONCLUSIONS

In this paper we have presented an analytical solution that can be used to calculate the temperature response of arrays of earth basket spiral ground heat exchangers. The analytical solution used is based on the well-known Finite Line Source equation that is extensively used in the simulation and design of vertical borehole, horizontal, Slinky[tm] and now also earth basket spiral heat exchangers. For the first time this allows a consolidated engineering ground source heat exchanger toolkit allowing the simultaneous evaluation of all types of ground heat exchangers.

The analytical model was validated based on a combination of sand-box experiments and CFD computations. Validations calculations were performed for a relatively wide but realistic range of heat exchanger, soil and system operational parameters (heat exchanger pitch and radius, soil thermal conductivity and specific heat flux rate). Results show an overall very good agreement between the analytical solution and detailed CFD results. Further research will identify where improvements of the models are possible and will analyse the transient response of the different models.

REFERENCES

Blomberg, T., Claesson, J., Eskilson, P., Hellström, G. and Sanner, B. Earth Energy Designer v. 4,2 (2019).

Cimmino, M., Bernier, M. and Adams, F. A contribution towards the determination of g-functions using the finite line source. *Applied Thermal Engineering*. 51, (2013), 401-13.

Cui P, Li, X., Man, Y and Fang, Z. Heat transfer analysis of pile geothermal heat exchangers with spiral coils. *Appl. Energy*, 88 (2011), 4133-9.

Eskilson P. Thermal analysis of heat extraction boreholes. *Doctoral thesis. Lund University, Department of Mathematical Physics*. Lund, Sweden; 1987.

Kling, S., Haslinger, E., Lauermann, M., Witte, H.J.L., Reichl, C., Steurer, A., Dörr, C., Dragisa, P and Robin, F. Geofit: Experimental investigations and numerical validation of shallow spiral collectors as a bases for development of a design tool for geothermal retrofitting of existing buildings. *Proceedings of the European Geothermal Congress 2022*. Berlin, Germany. (2022).

Lei, F., Hu, P and Huang, X. Hybrid analytical model for composite heat transfer in spiral pile ground heat exchanger. *Appl. Thermal Eng*. 137, (2018), 555-66.

Li, H., Nagano, K. and Lai, Y. A new model and solutions for a spiral heat exchanger and its experimental validation. *Int. J. Heat. Mass. Transf.* 55, (2012), 4404-14.

Man, Y., Yang, H., Dao, N. Cji, P., Liu, L and Fang, Z. Development of spiral heat source model for novel pile ground heat exchangers. *HVAC R Res.,* 17(6) (2011), 1075-88.

Meeng, C.L., Development of an engineering tool for the design of novel shallow ground heat exchangers – GEOFIT. MSc Thesis. *Technical University of Eindhoven*. Eindhoven. (2020).

Park, S., Lee, S-R., Park, H., Yoon, S and Chung, J. Characteristics of an analytical solution for a spiral coil type ground heat exchanger. *Computer and Geotechnics*. 49, (2103), 18-24.

Spitler, J.D. 2000. GLHEPRO -- A Design Tool For Commercial Building Ground Loop Heat Exchangers. *Proceedings of the Fourth International Heat Pumps in Cold Climates Conference*, Aylmer, Québec. August 17-18. (2000).

Wang, D., Lu, L and Cui, P. A new analytical solution for horizontal geothermal heat exchangers with vertical spiral coils. *Int. J. Heat. Mass. Transf.* 100, (2016), 111-20.

Xiong, Z., Fisher, D.E. and Spitler, D. Development and validation of a Slinky[tm] ground heat exchanger model. *Applied Energy*. 141, (2015), 57-9.